JOURNAL OF AIRCRAFT
Vol. 31, No. 1, Jan.–Feb. 1994

Effect of Wind-Tunnel Walls on Airfoil Droplet Impingement

Michael B. Bragg* and Stephen L. Wells†
University of Illinois at Urbana—Champaign, Urbana, Illinois 61801

A two-dimensional computer code, capable of modeling wind-tunnel walls, was written to calculate the impingement of water droplets on an airfoil in an incompressible, inviscid flow. The calculated flowfield was validated by comparison to standard wind-tunnel wall correction methods. When run without the walls present, the calculated droplet impingement compared well to a free-air code. Once validated, the code was run for an NACA 4412 at several angles of attack, tunnel heights, and modified inertia parameters. The effect that the tunnel walls had on the local impingement efficiency and the total collection efficiency was examined. Additionally, changes in the limits of impingement and changes in the origin of tangent trajectories are discussed with applications to icing tunnel testing. The effects of the walls are found to be small for reasonable tunnel height-to-chord ratios due to canceling near- and far-field aerodynamic effects on the droplet. The effect on total collection efficiency changes sign when droplet diameter (modified inertia parameter) is increased due to a change in the relative importance of droplet inertia and drag.

Nomenclature

C_D = droplet drag coefficient
c = airfoil chord length
E = airfoil total collection efficiency
F_r = Froude number, $U/\sqrt{(cg)}$
g = gravitational acceleration constant
H = tunnel height
h = airfoil projected height
K = particle inertia parameter, $\sigma\delta^2 U/18c\mu$
K_0 = modified inertia parameter
R_u = droplet freestream Reynolds number, $\rho\delta U/\mu$
S = surface length nondimensionalized by airfoil chord length
t = time
U = tunnel speed
$\mathbf{u}$ = local flowfield velocity
u = component of the local air velocity in the x direction
v = component of the local air velocity in the y direction
x = global x coordinate
y = global y coordinate
α = airfoil geometric angle of attack
β = local impingement efficiency
δ = droplet diameter
η = droplet nondimensional position
ρ = air density
σ = droplet density
τ = nondimensional time, Ut/c
Ψ = stream function

Subscripts
AF = on or of the airfoil
LW = on or of the lower wall
UW = on or of the upper wall

Superscripts
$\bar{}$ = vector quantity
$\dot{}$ = first derivative with respect to τ
$\ddot{}$ = second derivative with respect to τ

Introduction

AIRCRAFT operating in icing conditions can form ice accretions on the leading edges of lifting surfaces. This may lead to large aerodynamic penalties in lift and drag. In order to prevent this, deicing or anti-icing systems have traditionally been employed on aircraft. These systems tend to be relatively heavy, result in high power usage, or require significant maintenance. Because of this, the size of the system must be kept to a minimum. Only key elements of the structure such as the lifting surfaces and engine inlets can be protected. Even on these surfaces, the only portions which are normally protected are the portions of the leading edge where the supercooled water droplets are expected to impinge and form ice.

In an effort to predict where the water droplets will impinge on an airfoil, several computer codes have been written.[1–5] Special wind-tunnel tests have been conducted, primarily in icing tunnels, in an effort to directly measure droplet impingement characteristics for code validation.[6,7] However, most existing codes calculate the impingement efficiency in free air, while wind-tunnel tests are affected by the presence of the wind-tunnel walls. The effects of wind-tunnel walls on airfoil aerodynamics has been extensively studied[8]; however, the effect that wind-tunnel walls have on airfoil droplet impingement is relatively unknown. In order to use experimental wind-tunnel data to validate free-air computational methods, the wall effects must be understood.

This article reports an exploratory computational study of the effect of wind-tunnel walls on two-dimensional airfoil droplet impingement characteristics. The computer program was developed from Bragg's two-dimensional free-air droplet trajectory code.[1] The flowfield was replaced with an airfoil vortex panel code, originally written by Lowrie,[9] modified to include the capability to model wind-tunnel walls. Using this code, the effect that wind-tunnel walls have on droplet trajectories and impingement characteristics was examined. An extension

Presented as Paper 92-0642 at the AIAA 30th Aerospace Sciences Meeting, Reno, NV, Jan. 6–9, 1992; received Feb. 25, 1992; revision received Feb. 14, 1993; accepted for publication March 10, 1993.

*Associate Professor, Department of Aeronautical and Astronautical Engineering, 306 Talbot Laboratory, 104 S. Wright St. Associate Fellow AIAA.

†Graduate Research Assistant, Department of Aeronautical and Astronautical Engineering; currently Engineer/Scientist, Aerodynamics Technology, Transport Aircraft Unit, McDonnell Douglas Aircraft, Mail Code 36-41, 3855 Lakewood Blvd., Long Beach, CA 90846. Member AIAA.

of these results could find application in correcting wind-tunnel droplet trajectory data to the free-air case.

Theoretical and Numerical Method

Flowfield

The inviscid flowfield method chosen uses vortex panels with linearly varying strength to model the flow about a two-dimensional airfoil, either in a wind tunnel or in free air. Using an established panel method,[9] modifications were made to add tunnel walls to the code. Airfoil coordinates are input to the program, thus defining the geometry of the panels used to model the airfoil. The airfoil is then rotated to the specified angle of attack with respect to the global coordinate system. When tunnel walls are to be included, the code requires the length of the computational wind-tunnel "test section" ahead of the leading edge. This length is then added behind the leading edge to give an effective test section length. A computational test section length of 10 airfoil chord lengths was used for all the calculations in this article. Constant length panels were used on the wind-tunnel walls for simplicity. Figure 1 shows an NACA 4412 airfoil in the computational tunnel.

Knowing the geometry of each wall and airfoil panel, the vortex strength at the end points of each panel can be calculated. To do this, the value of Ψ is assumed constant but unknown on the airfoil. On each wind-tunnel wall Ψ is constant and is given a value equal to the vertical distance from the global origin. The governing equation is then

$$-\Psi_{\text{body}} + \sum_{j=1}^{N} K_{ij}\gamma_j = -y_i$$

Here, K_{ij} is an influence coefficient, and γ_j is the strength of the vortex panel j at its end point. Ψ_{body} is the value of the stream function on the body at control point i whose global vertical coordinate is given by y_i. In this instance, Ψ_{body} can be Ψ_{AF}, Ψ_{UW}, or Ψ_{LW}, depending upon the body to which the ith control point belongs. In this method, the end points of each panel serve as the control points.

The influence coefficients[9,10] and the values of Ψ on the upper and lower wall can be calculated from the known geometry. By inverting the influence coefficient matrix (Fig. 2) and multiplying by the right side vector, the vortex strengths as well as the value of Ψ on the airfoil can be found.

Having solved for the vortex panel strengths at the given angle of attack, the velocity at any point in the flowfield can be calculated. Whenever the ordinary differential equation solver in the trajectory portion of the code requests u and v at some location, the code computes the stream function at grid points centered on this location in the flow. A simple finite difference is then used to compute the velocities. Based on a brief study of the accuracy of the resulting velocity, the grid points are set 0.00001 chord lengths above, below, upstream, and downstream of the requested location.

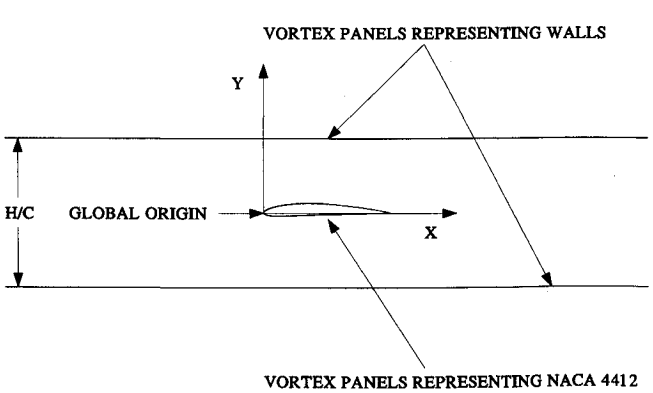

Fig. 1 NACA 4412 in computational wind tunnel.

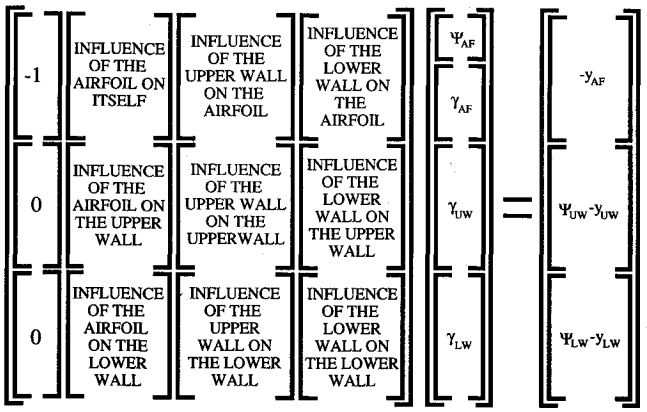

Fig. 2 Matrix equation for the flowfield solution.

Particle Trajectory

Once the velocity components of the local flowfield are known, the trajectory of the particle can be obtained by using the following trajectory equation[11]

$$\ddot{\bar{\eta}} = \frac{1}{K}\left(\frac{C_D R}{24}\right)\left(\frac{\bar{\mathbf{u}}}{U} - \dot{\bar{\eta}}\right) + \frac{1}{F_r^2}\frac{\bar{g}}{g}$$

R is given by

$$R = R_u\left|\frac{\bar{\mathbf{u}}}{U} - \dot{\bar{\eta}}\right|$$

It has been shown[11] that K and R_u can be combined into a single similarity parameter K_0, which simplifies data presentation and reduces the number of variables. K_0 is given by

$$K_0 = 18K\left[\frac{1}{R_u^{2/3}} - \frac{\sqrt{6}}{R_u}\arctan\left(\frac{R_u^{1/3}}{\sqrt{6}}\right)\right]$$

The drag coefficient of the droplet is calculated by the method of Langmuir and Blodgett.[12] Given R_u, F_r, K, the droplet initial conditions, and the airfoil-tunnel geometry, the trajectory equation can be solved by the method of Gear.[13] This method uses a predictor-corrector scheme with variable step size suitable for stiff systems. Individual droplet trajectories can be calculated and impingement characteristics can be computed.

The local impingement efficiency, $\beta = dy_0/dS$, is a nondimensional mass flux of impinging droplets at a point on the airfoil. Here, y_0 is the starting y location of an impinging droplet far ahead of the airfoil, and S is the surface length of the impact location from the leading edge of the airfoil. The code then runs a series of droplet trajectories, fits a cubic spline through the y_0 vs S data points of the impinging droplets, and then computes the slope of the spline at a series of surface positions. This slope is then β at that surface location.[1]

The airfoil total collection efficiency is defined as $E = \Delta y_0/h$. Here, Δy_0 is the initial y distance between the two tangentially impinging droplets. The projected height of the airfoil perpendicular to the freestream direction is h.

Code Validation

Validation of the computational method was done in two steps. First, the ability of the code to properly model the effects of wind-tunnel walls was examined. The program was run for the case of an NACA 4412 at 4-deg angle of attack. The wind-tunnel height was then varied from 1 to 3 chord lengths, and a no wall case was run. Two-dimensional wall correction methods from Rae and Pope[8] were then applied. The corrections were limited to the solid body blockage correction and streamline curvature correction for lift, both of

which the vortex code models. The wake blockage correction was ignored since the panel code does not simulate wake blockage.

The two methods show very similar lift increases due to the presence of the walls for a given height to chord ratio. In Fig. 3, ΔC_l is given by

$$\Delta C_l = C_{l_{\text{withwalls}}} - C_{l_{\text{nowalls}}}$$

The small differences that do exist between the two methods can probably be attributed to the crude single lumped vortex model used to simulate streamline curvature in the wall correction method of Ref. 8.

The next stage of the validation is to show that the present computational method predicts trajectories and impingement characteristics accurately. This was done by comparing the computational results on an NACA 4412 at 4-deg angle of attack at a K_0 of 0.057 to an already validated code.[1] In order to accurately calculate the flowfield, 200 vortex panels were used to model the NACA 4412 airfoil. The panels were packed closely in the area of the leading edge to ensure that the flow in this area was calculated correctly. When cases were run with tunnel walls, 90 panels were used on both the upper and lower walls. It can be seen from Fig. 4 that the predicted β curves are nearly identical when the dense panel distribution was used in the present method. The present method shows a slight shift in impingement to the lower surface which indicates a slightly higher predicted lift coefficient at $\alpha = 4$ deg.

Results and Discussion

Confident that the present method predicts both the flowfield and droplet trajectories accurately, the effect of wind-tunnel walls on droplet trajectories was studied using the program. An NACA 4412 was tested at various angles of attack, tunnel heights, and K_0 in order to evaluate the tunnel wall effects on droplet impingement. K_0 of 0.025 and 0.057 were

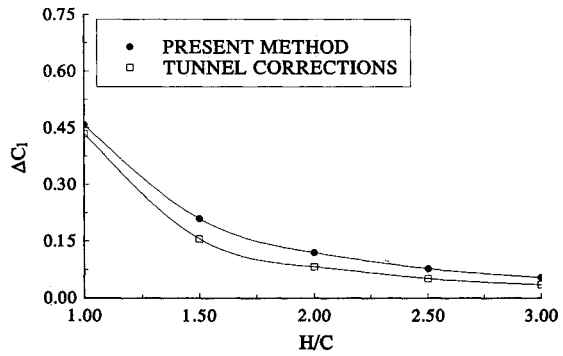

Fig. 3 Lift increase for an NACA 4412 at $\alpha = 4$ deg for various tunnel heights as predicted by tunnel wall corrections and the present method.

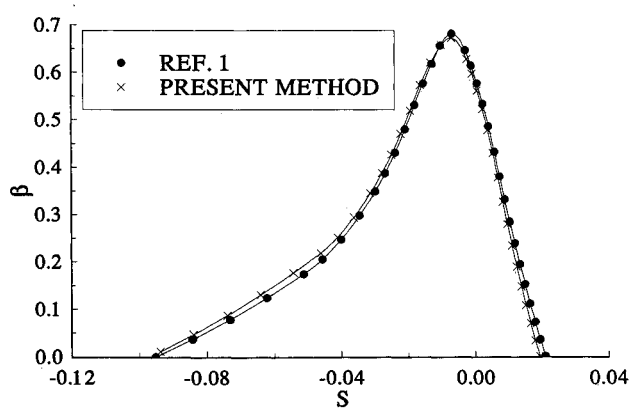

Fig. 4 Comparison of beta curves as calculated by the present method and Ref. 1 for K_0 of 0.057 and $\alpha = 4$ deg.

Table 1 Test conditions giving rise to K_0 of 0.025 and 0.057

K_0	Temperature, °F	Pressure, lb/ft²	U, ft/s	Droplet diameter, μm	Chord, ft
0.025	25	1975	240	15.7	3
0.057	25	1975	240	26.2	3

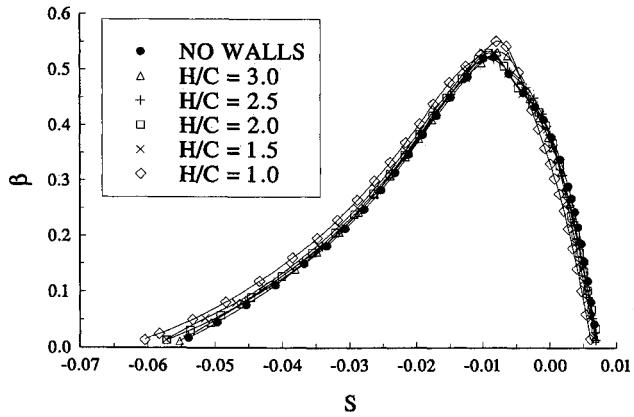

Fig. 5 Beta curves for the test conditions of $K_0 = 0.025$ and $\alpha = 4$ deg.

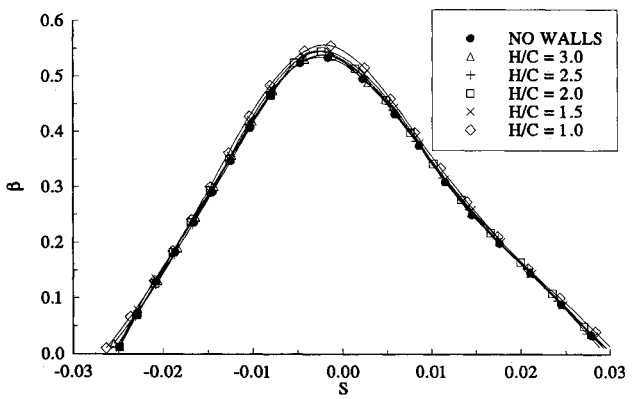

Fig. 6 Beta curves for the test conditions of $K_0 = 0.025$ and $\alpha = 0$ deg.

selected for the majority of the test runs. The approximate test conditions corresponding to these K_0 values can be found in Table 1. A few cases at higher K_0 are also reported.

Wall Effects at Low K_0

The effect of tunnel walls on the local impingement efficiency is small compared to the effect on the airfoil lift for all of the conditions tested. Comparisons were made on the NACA airfoil at K_0 of 0.025 and 0.057; α of 0, 4, and 8 deg; and H/C = 1, 1.5, 2, 2.5, 3, and free air. Examination of Figs. 5 and 6 show that regardless of the location of the walls, the β curves are qualitatively similar. The computational results shown in these figures are representative of the other cases as well.

The encroaching walls cause a greater $\beta_{\max}$ and increase the value of β on the lower surface of the airfoil at positive angles of attack. In Fig. 5, $\beta_{\max}$ is increased by 0.035 and β on the lower surface increases by as much as 0.03 for $H/C = 1$. This is also reflected in the limits of impingement on the upper and lower surface of the airfoil which show only a small change due to the height of the tunnel walls. From Fig. 5, a slight movement downstream of the lower surface limit of impingement from $S_l = -0.05526$ to $S_l = -0.06041$ as H/C changes from 3.0 to 1.0 is seen. Even less effect of tunnel height on the impingement limits is seen at the higher K_0 of 0.057. This small change in β is also reflected in the total collection efficiencies. As the walls come closer to the airfoil, more par-

ticles are forced to impinge upon the airfoil, resulting in a slightly higher value of E.

The percent increase in E due to the encroaching walls is given by

$$\% \text{ increase in } E = 100(E - E_\infty)/E_\infty$$

Here, E_∞ is the total collection efficiency with no walls present. As shown in Figs. 7 and 8, the change in E is only about 5–7% for the extreme case of $H/C = 1$. Note from Fig. 3 the effect of the tunnel walls at $H/C = 1.0$ on the airfoil lift is a 46% increase. In more conventional situations where $H/C > 2$, the change in total collection efficiency is reduced to less than 2%. The present computer code has a user selectable precision variable used in the calculation of the collection efficiency. It controls the iteration process of finding the tangent trajectories, and therefore controls the precision to which the collection efficiency is calculated. In all runs, precisions of 0.25% of the calculated values of E were used.

The effect of angle of attack on the collection efficiencies shows no discernable trend for the lower K_0 runs. For the higher K_0 case shown in Fig. 8, higher angles of attack do show a small but noticeable increase in the change of collection efficiency.

In an attempt to better understand the effect of the walls, the droplet trajectories themselves were studied. Figure 9 shows the paths of the upper and lower tangent trajectories for particles with a K_0 of 0.025. The NACA 4412 is at 4-deg angle of attack, and various tunnel heights are shown.

The starting location of an impinging particle differs by as much as 15% chord with changing tunnel height. However, the plots show that all the particles seem to become entrained into the same path as they draw near to the airfoil. This is most likely due to two factors. The first factor is that the

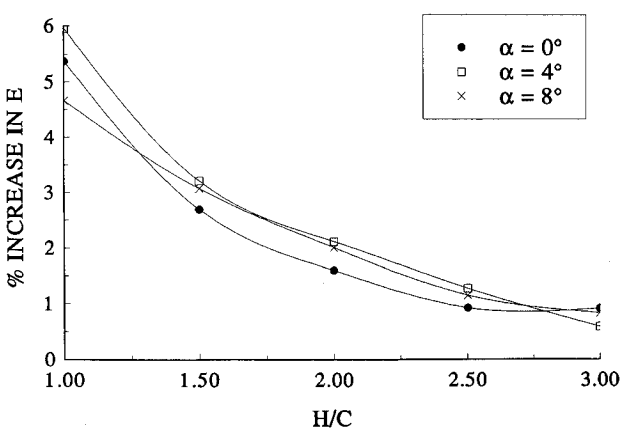

Fig. 7 Total collection efficiency increase for various α and H/C for $K_0 = 0.025$.

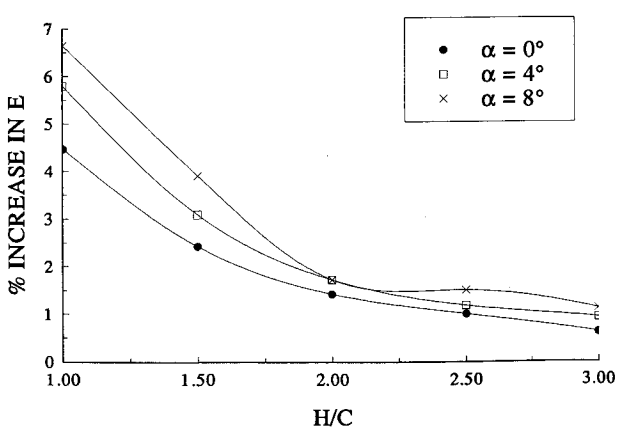

Fig. 8 Total collection efficiency increase for various α and H/C for $K_0 = 0.057$.

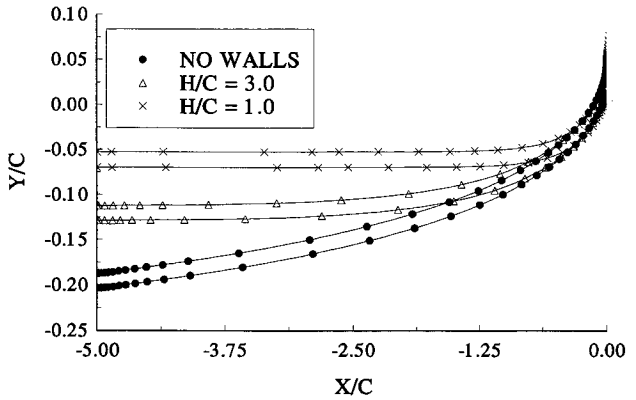

Fig. 9 Upper and lower tangent trajectories for three tunnel heights with $K_0 = 0.025$.

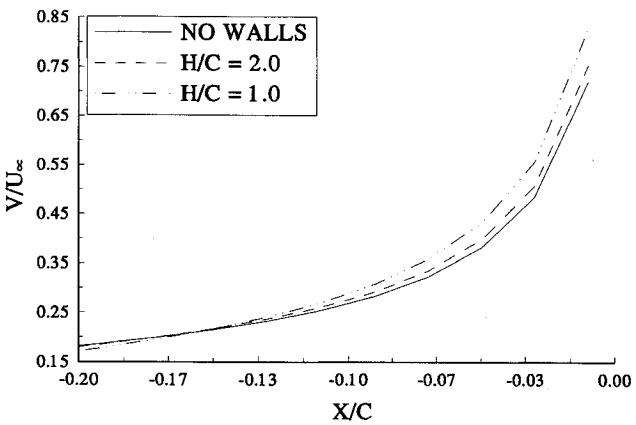

Fig. 10 Near-field upwash seen 5% chord above the centerline of the tunnel for various tunnel heights.

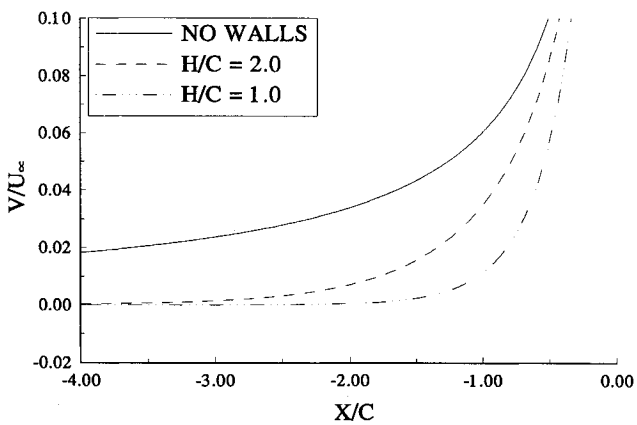

Fig. 11 Far-field upwash seen 5% chord above the centerline of the tunnel for various tunnel heights.

wind-tunnel walls restrict the far-field streamlines, and the second is that the velocity gradients near the leading edge of the airfoil increase with reduced wall spacing. Far away from the airfoil, the particles in the tunnel travel on a much more linear path due to the upwash reduction imposed by the tunnel walls. However, as it approaches the leading edge of the airfoil, the particle encounters increased velocity gradients that are a product of the increased airfoil circulation created by the proximity of the walls to the airfoil. Although the upwash decreases in the far field as the walls get closer together, the upwash increases in the near field. Figures 10 and 11 show the vertical component of velocity in the airfoil near field and far field just above the centerline of the tunnel.

The two effects seem to cancel one another. The far-field effect acts like a circulation or effective angle-of-attack decrease, while the near-field effect acts as a circulation or ef-

fective angle-of-attack increase. The increased vertical velocities near the leading edge increase the drag force on the particle. This increased drag force is enough to accelerate the droplets from their restricted paths into nearly the same trajectory, regardless of the tunnel height. This then explains why the collection efficiencies and impingement efficiencies do not change significantly with changes in tunnel height for this range of K_0.

An additional source of concern is the location in the tunnel from which the impinging droplets originate. Figure 9 shows a 15% chord change in the droplet starting location for the $H/C = 1.0$ case. It is difficult to maintain uniform cloud properties over a large cross-sectional area of the tunnel, and errors can result when impinging droplets come from outside this sometimes small region. This may be a legitimate concern for tunnels with small regions of uniform spray testing large models.

Wall Effects at High K_0

The effect of tunnel walls does not always increase the collection efficiency. In a limited investigation of the effect of K_0 on E, with and without walls, the effect of increasing E with encroaching walls was seen to reverse. In Fig. 12, it can be seen that for large K_0, the walls reduce the collection efficiency by the same order of magnitude that the walls increased E in the lower K_0 range. The same near- and far-field effects which explain the increase in E at low K_0, can also be used to explain the high K_0 result.

It has been shown for the free-air case that there exists a range of K_0 values which produce collection efficiencies greater than one.[14] This occurs because the upwash in the far field imparts sufficient momentum to the large, high K_0 droplets that there is neither sufficient time nor drag force in the airfoil near field to counter the upward momentum of the droplet.

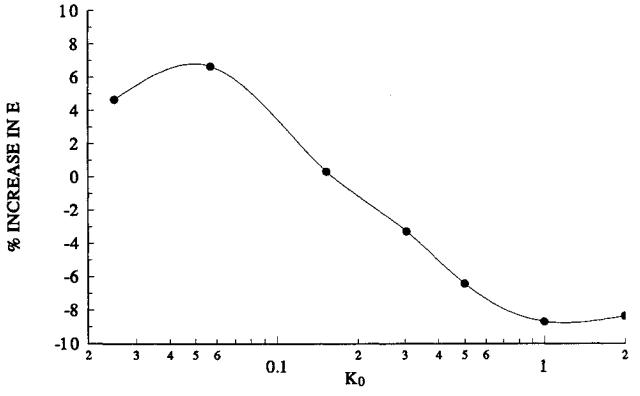

Fig. 12 Percent increase in E for an NACA 4412 at $\alpha = 8$ deg and $H/C = 1.0$.

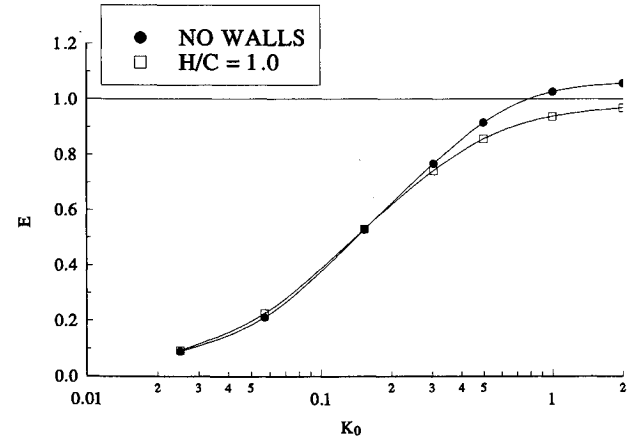

Fig. 13 Effect of K_0 and tunnel height on the collection efficiency of an NACA 4412 at $\alpha = 8$ deg.

Therefore, the droplet is presented with a larger airfoil projected height in the droplet trajectory direction than the airfoil projected height presented in the freestream direction. By imposing wall restrictions to cases with K_0 in this range, the far-field upwash is greatly reduced, thus reducing the upward momentum imparted to the drop. Without this upward momentum, the effective projected height presented to the particle is reduced, and the high K_0, high inertia particles cannot respond to the high-velocity local flowfield. This then would produce an E of less than 1. This is precisely what happens as can be seen in Fig. 13. From Fig. 12 note that the error in E is seen to decrease as K_0 becomes very small or very large. This is as expected, since at $K_0 = 0$ or ∞, E approaches 0 or 1.0, respectively, regardless of the presence of the tunnel walls.

Conclusions

The effect of wind-tunnel walls on airfoil droplet impingement was studied using a computational model. A computer code was written to compute droplet trajectories about a two-dimensional airfoil in a wind tunnel. A surface vortex panel code with linear strength variation was used to model the flowfield. The present method compared well to an existing droplet impingement code when no tunnel walls were used, and it predicted lift increases comparable to standard wind-tunnel wall lift corrections.

The effect of tunnel walls on droplet impingement was small, as compared to the effect on airfoil lift, regardless of the tunnel height-to-chord ratio. When H/C was less then 2.0, small increases on the order of 0.01 were seen in β_{max} and the value of β on the lower surface. Changes in the limits of impingement and in total collection efficiency were also well within the accuracy of current experimental techniques, where β is measured to within 10%.

At low K_0, less than about 0.13, the presence of tunnel walls increases the total impingement efficiency by no more than 7% for the cases studied. This seems to be due to a canceling effect of decreased upwash in the far field and increased upwash in the near field. The small K_0 droplets follow the streamlines very well and are initially restricted by the tunnel walls to a higher trajectory approaching the airfoil which is similar to a reduced airfoil circulation case. This is then compensated for in the near field by the increased airfoil circulation, and therefore, higher flowfield velocities. The end result is a canceling effect and very little influence of wind-tunnel walls on droplet impingement parameters. However, larger droplets have more inertia, which more heavily weights the far-field influence, and the result is a slight decrease in impingement parameters.

The droplet parameters examined here are typical of most two-dimensional airfoil droplet impingement experiments. Because the tunnel effects lie within the range of current experimental error, the failure to account for tunnel walls in past experiments and code validation has not been recognized. In fact, for the range of airfoil and droplet parameters examined here, and for a reasonable tunnel height-to-chord ratio, the wall effects are so small they may be ignored in most cases.

It should be noted that because the small effects seen here are due to a balance in the near- and far-field tunnel wall effects, the results may be different for other test conditions where the balance may be different. Three-dimensional tests such as wing and engine inlet tests warrant further investigation, as they were not addressed by this study. The results of this analysis of tunnel wall effects on airfoil droplet impingement have been encouraging, but an expanded study with experimental verification of the computational results is needed before a reliable wall correction scheme can be implemented.

References

[1]Bragg, M. B., "Rime Ice Accretion and Its Effect on Airfoil Performance," Ph.D. Dissertation, Ohio State Univ., Columbus, OH,

1981; see also NASA CR 165599, March 1982.

[2]Norment, H. J., "Calculation of Water Drop Trajectories to and About Arbitrary Three-Dimensional Bodies in Potential Airflow," NASA CR 3291, 1980, March 1982.

[3]Gent, R. W., "Calculation of Water Droplet Trajectories About an Aerofoil in Steady, Two-Dimensional, Compressible Flow," Royal Aircraft Establishment TR 84060, June 1984.

[4]Lozowski, E. P., and Oleskiw, M. M., "Computer Modeling of Time-Dependent Rime Icing in the Atmosphere," Cold Regions Research and Engineering Lab. 83-2, Jan. 1983.

[5]Ruff, G. A., and Berkowitz, B. M., "User's Manual for the NASA Lewis Ice Accretion Prediction Code (LEWICE)," NASA CR-185129, May 1990.

[6]Gelder, T. F., Smyers, W. H., and Von Glahn, U., "Experimental Droplet Impingement on Several Two-Dimensional Airfoils with Thickness Ratios of 6 to 16 Percent," NACA TN 3839, Dec. 1956.

[7]Papadakis, M., Elangonan, R., Freund, G. A., Jr., Breer, M., Zumwalt, G. W., and Whitmer, L., "An Experimental Method for Measuring Water Droplet Impingement Efficiency on Two- and Three-Dimensional Bodies," NASA CR 4257, Nov. 1989.

[8]Rae, W. H., Jr., and Pope, A., *Low-Speed Wind Tunnel Testing*, Wiley, New York, 1984.

[9]Lowrie, R., "An Airfoil Design Procedure for Reducing the Effect of Surface Contamination on Laminar Flow Airfoils," M.S. Thesis, Ohio State Univ., Columbus, OH, 1986.

[10]Soinne, E., and Laine, S., "An Inverse Boundary Element Method for Single Component Airfoil Design," *Journal of Aircraft*, Vol. 22, No. 6, 1985, pp. 541–543.

[11]Bragg, M. B., "A Similarity Analysis of the Droplet Trajectory Equation," *AIAA Journal*, Vol. 20, No. 12, 1982, pp. 1681–1686.

[12]Langmuir, I., and Blodgett, K., "A Mathematical Investigation of Water Droplet Trajectories," Army Air Forces TR 5418, Feb. 1946.

[13]Gear, C. W., "DIFSUB for Solution of Ordinary Differential Equations," *Communications of the Association for Computing Machinery*, Vol. 14, March 1971, pp. 785–790.

[14]Bragg, M. B., and Gregorek, G. M., "An Incompressible Droplet Impingement Analysis of Thirty Low and Medium Speed Airfoils," Ohio State Univ., Aeronautical and Astronautical Research Lab. TR 8202, Columbus, OH, Feb. 1982.